Nanoscale

Nanoscale

COMMUNICATION

3D Printing of Multifunctional Nanocomposite Helical Liquid Sensor

Shuang-zhuang Guo, [a] Xuelu Yang, [a] Marie-Claude Heuzey[b] and Daniel Therriault [a]

A multifunctional 3D liquid sensor made of a PLA/MWCNT nanocomposite and shaped as a freeform helical structure was fabricated by solvent-cast 3D printing. The 3D liquid sensor featured a relatively high electrical conductivity, the functionality of liquid trapping due to its helical configuration, and an excellent sensitivity and selectivity even for a short immersion into solvents.

Conductive polymer nanocomposites (CPNs) with relatively low loading of conductive nanofillers such as graphene,[1] carbon nanotubes (CNT),[2] and silver nanowires[3] can benefit from multifunctional properties such as high mechanical strength and stiffness, thermal and electrical conductivity. Those properties make CPNs suitable for a broad range of applications such as sensors,[4] actuators,[5] electromagnetic interference shielding,[6] as well as energy and gas storage.[7] Among these applications, CPNs have been used for various types of sensors based on the polymer reaction to environmental changes, which affects the electrically conductive nanofiller network.[8-10] External stimuli such as temperature shift,[11] mechanical deformation,[12] and the presence of gases and vapors[13] or solvents[14] can lead to measurable electrical resistance changes of the CPNs. For example, CPNs can be used as liquid sensors since the presence of organic liquids can result in the local disconnection of electrical contacts between individual nanoparticles.[15-17] These sensory structures can provide reliable and locally resolved analysis of organic solvent leakages of tanks in ships and trucks or piping systems, or volatile organic compound detection and discrimination in air quality monitoring.[18] A few manufacturing techniques have been reported to fabricate liquid sensors such as melt spinning,[16] and compression molding.[19, 20] However, the geometries of liquid sensors are limited to unidirectional (1D) fibers,[16] planar (i.e., two-dimensional, 2D) films[19-21] and textiles[18] , and their size are of the order of centimetres (2-30 cm), which lack portability and demand high power consumption.

CPNs-based sensors could benefit from the ability to pattern micro-sized features in complex three-dimensional (3D) architectures. The 3D printing technique allows functional inks to be precisely patterned in filamentary form into various geometries.[22, 23] For example, thermoset polymers and their nanocomposites have been employed in UV-assisted 3D printing to fabricate microcoils[24] and strain sensors.[4] Also, a thermoplastic polymer, polylactide (PLA), has been used in solvent-cast 3D printing to build various microsystems including microstructured fibers, helical fluidic microchannels and copper plated micro-antennas.[25, 26]
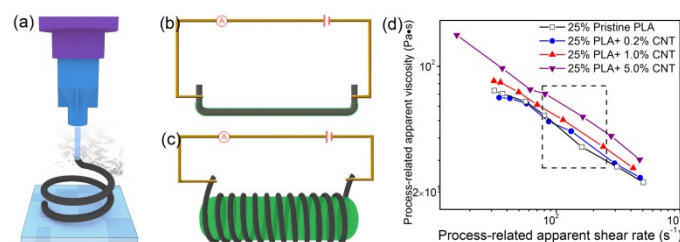

Figure 1. (a) Schematic representation of the solvent-cast 3D printing of nanocomposite microstructures. Schematic circuits of the liquid sensing test for (b) the straight line sensor and (c) the 3D helical sensor. (d) Process-related apparent viscosity of PLA nanocomposite solutions (typical processing window used in this work is shown by the dashed box).

In the present work, PLA/multi-walled carbon nanotubes (MWCNT) solutions were developed to fabricate a helical liquid sensor in a freeform fashion using the solvent-cast 3D printing technique (**Figure 1**a). This original nanocomposite microstructure can exhibit multifunctional properties such as electrical functions (e.g., conductivity, strain sensitive resistivity), and structural functions (e.g., liquid trapping, light weight, compactness), which make it an ideal candidate for liquid sensing applications. The inks were prepared by dissolving a masterbatch of the PLA/MWCNT nanocomposite prepared in the molten state in a low boiling point solvent (dichloromethane, DCM). The nanocomposite solutions were then loaded in a syringe and extruded from a micronozzle under a specific constant pressure. The rigidity of the extruded filament rapidly changed from fluid-like to solid-like due to rapid solvent evaporation, which could lead to highly accurate freestanding features, when using the appropriately adjusted

process parameters and ink properties, similar to the approach described before.[26] Two geometries, a 1D straight line (for sake of comparison) and a freeform 3D helix, were fabricated and tested as liquid sensors (see Figure 1b,c).

The process-related viscosity of the nanocomposite inks is critical, since it determines its flowing behavior inside the nozzle and the initial rigidity of the extruded filament. The CPNs-based inks exhibited shear-thinning, and the magnitude of the process-related apparent viscosity with respect to neat PLA was increased for MWCNT loading of 1 wt% and above (Figure 1d). The apparent viscosity of the ink with 5 wt% MWCNT loading was 40% higher than that of the neat PLA ink (Figure 1d), resulting in extruded filaments that were more rigid and which facilitated the fabrication of 3D self-supporting structures. Hence, the 5 wt% MWCNT ink could successfully be used to fabricate the 3D freeform helix (**Figure 2**a, and Supporting Information, Movie 1) using a 150 μm inner diameter nozzle, and the typical applied pressures were between 1.4 to 2.5 MPa, which correspond to process-related shear rates of $\sim$ 80 - 220 s^{-1} (dashed box in Figure 1d).
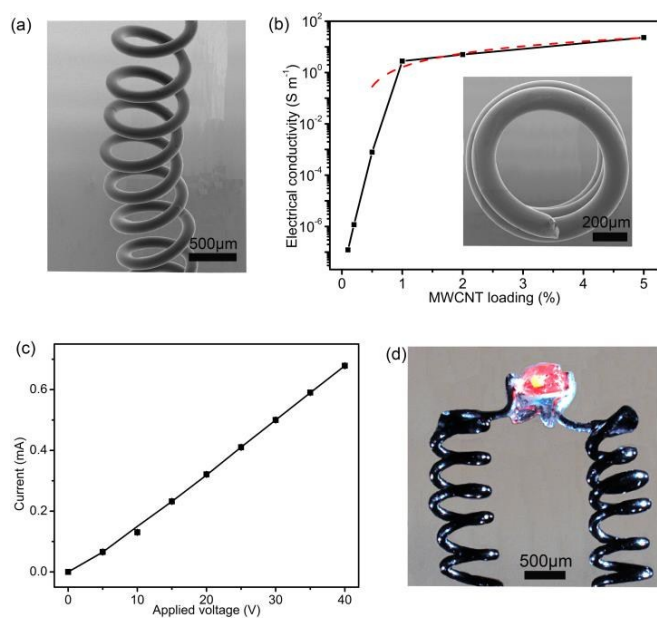

Figure 2. (a) Inclined side view SEM image of the nanocomposite helix. (b) Electrical conductivity of PLA nanocomposite as a function of MWCNT loading. The dashed line is a power-law expression fit[27] and the inset is a top view SEM image of the nanocomposite helix. (c) Measured current upon applied voltage between two ends of the 3D helical sensor. (d) Optical image of two helical sensors mechanically supporting and electrically sourcing a luminous LED bulb.

The electrical properties of the fabricated helix are critical in the case of sensing applications. In this solvent-cast 3D printing approach, the electrical conductivities of the extruded nanocomposite filaments showed typical concentration percolation behavior with increasing MWCNT loadings, and the electrical percolation threshold was found to be approximately 0.3 wt% (Figure 2b) after fitting the data using a power-law expression.[27] In order to compensate for variation of filler orientation due to processing and changes in resistivity, the filler level should be well above the percolation threshold for sensing applications.[28] In the present work the nanocomposite straight line and 3D helix were fabricated using a 30 wt% PLA in a DCM solution with 5 wt% MWCNT loading, approximately one order of magnitude above the

percolation threshold. The measured current-voltage curve for the printed 3D helix (Figure 2c) showed that its electrical conductivity was about 23 S m^{-1}. Finally to demonstrate that the helix exhibited adequate mechanical stiffness and electrical conductivity, a small LED bulb (weight of 2.5 mg) could be fully lighted up under an applied voltage of $\sim$30 V (Figure 2d) while being supported by two fabricated helixes.

The driving mechanisms in polymer/CNT nanocomposites liquid sensor are polymer matrix swelling, due to the solvent molecule penetration, and resultant disconnection of the conductive CNT network.[19] The corresponding change of resistivity is thereby related to the local volumetric solvent absorption. When a dry CPN sensor specimen is immersed into a solvent, the swelling process starts at the material's surface and gradually develop into its core region.[18] Thus, the electrical response of the sensor depends on its geometry, the penetrating ability of the solvent and contact time.

Table 1. Characteristics of PLA and solvents used for sensing experiments.[29]

Material	Solubility parameter δT (MPa0.5)	Boiling point (°C)	Vapor pressure (kPa, 20 °C)	Molar volume (cm3 mol-1)	Flory-Huggins interaction parameter χ_{12}
Polylactide	21.2	-	-	-	-
Acetone	19.9	56.2	24.6	73.4	0.05
Ethyl acetate	18.2	77.5	9.9	98.2	0.36
Toluene	18.2	110.6	2.9	105.9	0.39
Ethanol	26.6	78.4	5.8	58.4	0.70

The two different nanocomposite configurations (i.e., straight line and 3D helix) were characterized as liquid sensors in four different solvents (i.e., acetone, ethyl acetate, toluene, and ethanol) which were selected for their different solubility parameters, vapor pressures and molecular sizes (**Table 1**). The 3D helical sensor had a typical coil diameter of 1 mm and a length of 5 mm. The diameter of the extrudates was about 160 μm. The straight line sensor had similar filament diameter and linear length than the helix for comparison purposes. During short immersion tests, the sensors were cyclically immersed in a solvent at room temperature for 1 s, then taken out and left to dry in ambient air for 10 min. The change in electrical resistance of the sensors was monitored using a multimeter. In the case of the straight line sensor, a small amount of solvent remained on its surface when it was taken out of the liquid, as shown by fluorescent microscopy (**Figure 3**a). Thus the straight line sensor rapidly dried and 90% of the solvents evaporated within 10 - 40 s (Figure 3b), and hence allowed a very short contact time with the solvents. However for the 3D helical sensor, a large amount of liquid estimated at $\sim$3.9 mm^3 was trapped inside the structure after removal from the liquid. Figure 3c,d shows that the trapped liquid appears like a circular cylinder with a weight of $\sim$2.1 times that of the helix. As a result, the helical sensor took much longer to completely dry (100-360 s) (Figure 3d). The 3D helical sensor can greatly benefit from this structural function of liquid trapping, which provides a longer contact time with the solvent. The evaporation time of the four solvents was correlated to their respective vapor pressure (Table 1). In other words, a higher solvent vapor pressure corresponded to a faster evaporation rate. Hence, acetone evaporated the fastest (100 s), toluene took

the longest time to dry (360 s), and ethyl acetate (160 s) and ethanol (280 s) were in between the former two solvents.
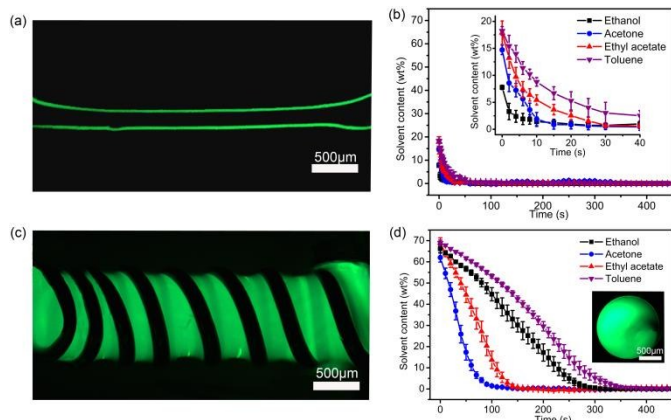

Figure 3. (a) Fluorescent microscopy side view image of a straight line sensor with liquid on its surface. (b) Solvent content as a function of time for the straight line sensor during drying process. (c) Fluorescent microscopy side view image of the liquid trapped in a 3D helical sensor. (d) Solvent content as a function of time for the 3D helical sensor during drying process (inset is a top view image of the helical sensor with fluorescent liquid trapped).

The penetrating ability of a solvent is mainly determined by its interaction with the polymer, which is expressed by the Flory-Huggins interaction parameter χ_{12} : $\chi_{12} = \dfrac{V_{sol}(\delta_{T\,pol} - \delta_{T\,sol})^2}{RT}$

$$(1)$$

where V_{sol} is the molar volume of the solvent, $\delta_{T\,sol}$ and $\delta_{T\,pol}$ are the solvent and polymer solubility parameters, respectively, T is the absolute temperature, and R is the ideal gas constant (R = 8.314 J K^{-1} mol^{-1}). The parameter χ_{12} was calculated for the various PLA/solvent pairs and is reported in Table 1. Low values of χ_{12} indicate strong interactions between the solvent and the polymer. Consequently, acetone ($\chi_{12} = 0.05$) exhibits the maximum penetrating ability in PLA, ethyl acetate ($\chi_{12} = 0.36$) and toluene ($\chi_{12} = 0.39$) are nearly equally second and ethanol ($\chi_{12} = 0.70$) has the lowest ability. Accordingly, amorphous PLA is reported to be soluble in acetone, swells in ethyl acetate and toluene, and is insoluble in ethanol.[29] During the short immersion cycling tests, the observed relative resistance change (R_{rel}) of the straight line sensor was inferior to 5 % for the four solvents (shown in **Figure 4**a). The reason is that the straight line had a small amount of solvent remaining on its surface, so that the solvents evaporated very fast without obviously swelling the polymer. Besides, the similar amplitudes of the R_{rel} for the four solvents indicate that the straight line sensor had no obvious selectivity to these solvents.

Compared to the straight line sensor, the liquid sensing behavior of the 3D helical sensor was quite different under the same short immersion cycling conditions (Figure 4b). Generally during each immersion / drying cycle, the R_{rel} sharply increased followed by a gradual decrease. The sharp increase was associated to the swelling of the polymer matrix when it was in contact with the solvent. After removal from the solvent, a given amount of solvent was trapped inside the 3D helical sensor, as mentioned before, which gradually evaporated. Thus, the resistance decreasing trend was gradual and in phase with the drying process. Specifically, the R_{rel} for toluene reached 15 % in a few seconds and decreased as the solvent evaporated.

Similarly, the maximum amplitudes measured for ethyl acetate and acetone were 13.7 and 9.4 %, respectively, as shown in Figure 4c as function of solvent vapour pressure and Flory-Huggins interaction parameter. Hence, the helical sensor was approximately three times more sensitive than the straight line sensor to these three solvents. However, the low response amplitude for ethanol ($\sim$ 1.6 %) was similar to that of the straight line sensor. The significant different responses for the four solvents mean that the helical sensor was selective even for very short contact time. This enhanced behavior can be explained by the solvent trapping feature of the 3D helix, which prolongs the solvent interaction with the polymer. Therefore, the sensing behavior could be controlled by both the Flory-Huggins interaction parameter χ_{12} and solvent evaporation behavior (Table 1 and Figure 4c). Since ethanol is a poor solvent for PLA, the polymer matrix just underwent light swelling[29] and the resistance of the sensor almost did not change. While for acetone, even though it is a good solvent for PLA, the amplitude of the relative resistance change (9.4%) was smaller than that for toluene and ethyl acetate, most probably because the faster evaporation of acetone (higher vapor pressure) led to shorter polymer contact time. In addition, the sensing behavior also exhibited an excellent repeatability during the five cycles tested. Similar experiments were repeated on a half filament-length helical sensor and the results showed that this different configuration had no obvious effects on the electrical response (Figure S1). This is expected since the geometry is the same, hence the relative amount of trapped liquids to the sensor length is similar, and so is the relative resistance change.
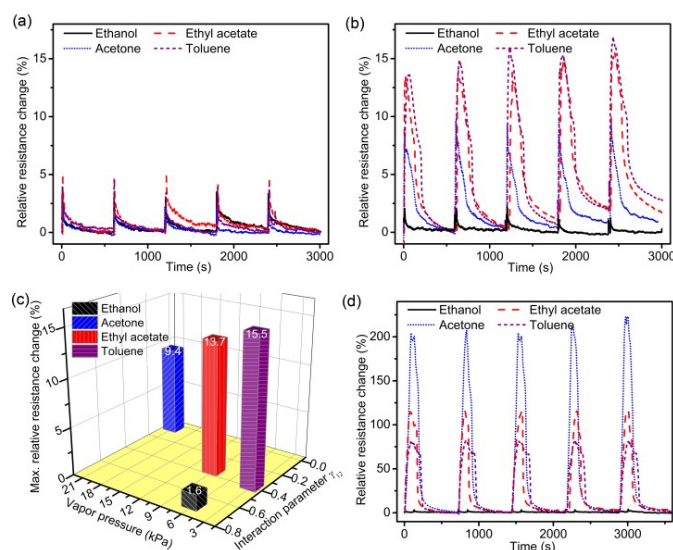

Figure 4. Relative electrical resistance change of (a) the straight line and (b) 3D helical sensors at short immersion cycles of (1 s) / drying (600 s) with four solvents. (c) Effect of vapor pressure and Flory-Huggins interaction parameter on the maximum relative resistance change of the helical sensor in short immersion tests. (d) Relative electrical resistance change of a 3D helical sensor during long immersion cycles of (120 s) / drying (600 s) in four solvents.

However when longer immersion tests were performed, the selectivity and sensitivity of the 3D helical sensor were quite different. Figure 4d shows the R_{rel} of the helical sensor during five cycles of 120 s immersion in the four solvents followed by 10 min drying. The sensitivity of the sensor sharply increased, where the response amplitudes for the solvents toluene, ethyl acetate, and acetone were 81, 114, and 205 %, respectively,

while the amplitudes for ethanol only slightly increased to 3.5 %. This seems to indicate that the selectivity of the 3D helical sensor is mostly determined by the Flory-Huggins interaction parameter when in contact with a solvent for a longer time (120 s vs. 1 s).

In extra-long (~1 h) immersion tests, the electrical response kinetics of the sensors are also correlated with the Flory-Huggins interaction parameters (Figure S2), because the intensities of the sensor response are proportional to the values of this parameter (Table 1). Villmow et al. found that the electrical response of a polycarbonate-based sensor upon immersion into "good" solvents was governed by the solvents molecular size.[19] In other words, when the Hansen solubility parameters of the solvents were very close to each other, the selectivity of the sensor was determined by the solvent molar volume. This phenomenon is in agreement with our findings based on the expression of the Flory-Huggins interaction parameter, which contains the molar volume of the solvent (Eq. 1).

Conclusions

In summary, we designed and printed a 3D liquid sensor made of a PLA/MWCNT nanocomposite in a novel freeform helical geometry. The structural feature of liquid trapping prompted the helical sensor with excellent sensitivity and selectivity, even for short immersion time (1 s) in the solvents, where the sensing response was governed by a combination of the polymer/solvent interaction parameter and the solvent vapor pressure. On the other hand, a straight line sensor fabricated with the same printing technique had no obvious sensing ability in these short immersion tests. In addition, it was found that the sensing ability of the helix was mainly determined by the polymer/solvent interaction parameter in long (120 s) and extra-long (3600 s) immersion tests. Although the geometry of the sensor was not fully optimized and only four solvents were tested, we believe that this work opens new avenues for the 3D printing of sensing architectures from functional nanocomposite materials. This PLA/MWCNT multifunctional system not only possesses relatively high electrical conductivity, but also light weight, compactness and good mechanical stiffness, resulting in a structural capability fully integrated with sensing functions, which are desired for low power consumption devices. Furthermore, these devices may find widely diverse potential applications in micro- and nanoscale systems for precision measurements, human skins and person health monitoring, pollutants detection in natural environments and remote-controlled smart devices.

Experimental Section

PLA/MWCNT nanocomposite inks: As-received pellets of polylactide (PLA 4032D, Natureworks LLC) and multi-walled carbon nanotubes (MWCNT, NC7000, Nanocyl) were dried in a vacuum oven (G05053-10, Cole-Parmer Instrument Company) for 12 h at 50 ℃ before processing. The MWCNT had a typical diameter of 9.5 nm, average length of 1.5 μm and purity of 90 %, as stated by the manufacturer. First, the PLA pellets and 5.0 wt% of MWCNT were premixed and then fed into a micro-compounder (5 mL, DSM Xplore) at 170 ℃ and 100 rpm. After a mixing time of 5 min at 180 ℃ and 300 rpm, the masterbatch of the PLA nanocomposite was extruded as strands. Then, the inks were prepared by diluting the masterbatch with desired amount of neat PLA in dichloromethane (DCM, Sigma-Aldrich) to prepare nanocomposite solutions of 30 wt% PLA concentration and various MWCNT loadings (0.1, 0.2, 0.5, 1.0, 2.0, 5.0 wt%). After dissolving for 12 h, the solution inks were stirred and sonicated in an ultrasonic bath (Ultrasonic cleaner 8891, Cole-Parmer) for 1 h. The inks were then stored in sealed bottles until processing. The process-related apparent viscosities of the inks were calculated from constant-pressure capillary flow data as described elsewhere.[26]

Solvent cast 3D printing: The deposition system consisted of a computer controlled robot (I&J2200-4, I&J Fisnar) moving a dispensing apparatus (HP-7X, EFD) along the *x*, *y* and *z* directions. The nanocomposite solution inks were housed in syringes (3 mL barrel, EFD), which were attached to a micronozzle. The 1D straight line and 3D helical sensors were fabricated from the PLA/MWCNT 5 wt% nanocomposite solution using a micronozzle with a 150 μm inner diameter (5130-0.25-B, EFD) under an applied pressure of 1.75 MPa and 0.1 mm s^{-1} robot velocity. The length of the straight line was 5 mm and the diameter of the filament was ∼ 160 μm. The pitch of the helix was 0.5 mm and the radius of the coil was 0.5 mm. The morphology of the microstructures was characterized using optical microscopy (BX-61, Olympus) and SEM (JSM-7600F, JEOL. Ltd.).

Liquid evaporation tests: The drying behavior of the sensors was evaluated by resting the sensors on a high-precision balance (GH-202, A&D Engineering) right after immersion in the solvents. First, the straight line and 3D helical sensors were immersed in four different solvents (i.e., acetone, toluene, ethyl acetate, and ethanol) for 1 s. Then the wet sensors were hung on a metal holder on the precision balance for 10 min to record the weight change at room temperature. Following this recording period, the sensors were dried in an oven (G05053-10, Cole-Parmer) at 50 ℃ for 5 h and weighed again. The mass of the dried sensors was then used to calculate the real-time solvent content.

Liquid sensor tests: The liquid sensing capability of the sensors was monitored by recording the resistance change during several immersion / drying cycles at room temperature. The straight line and 3D helical sensors were hung up between two copper electrical probes separated by a distance of 5 mm. Only the nanocomposite sensor part was immersed in the liquid to keep the electrodes dry. The resistance was continuously monitored using a digital multimeter (6517B, Keithley), interfaced with Lab View software. Five short immersion (1 s) / drying (600 s) cycles were periodically performed on the straight line and helical sensors in four different solvents (i.e., acetone, toluene, ethyl acetate and ethanol). Another set of immersion tests in the form of longer cycles (120 s) / drying (600 s) were also carried on the helical sensor in the four solvents. The relative resistance change R_{rel} was calculated by dividing the difference between the actual resistance (R) and the initial resistance (R_i) by R_i.

Acknowledgements

Nanoscale Accepted Manuscript

Notes and references

[a] Laboratory of Multi-scale Mechanics, Mechanical Engineering Department
Research Center for High Performance Polymer and Composite Systems (CREPEC)
École Polytechnique de Montreal
C.P. 6079, succ. Centre-Ville, Montreal, QC H3C 3A7 (Canada)
E-mail: daniel.therriault@polymtl.ca
[b] Chemical Engineering Department
Research Center for High Performance Polymer and Composite Systems (CREPEC)
École Polytechnique de Montreal
C.P. 6079, succ. Centre-Ville, Montreal, QC H3C 3A7 (Canada)
Electronic Supplementary Information (ESI) available: [details of any supplementary information available should be included here]. See DOI: 10.1039/c000000x/

1. T. H. Seah and M. Pumera, Sens. Actuators, B, 2011, 156, 79-83.

2. J. Benson, I. Kovalenko, S. Boukhalfa, D. Lashmore, M. Sanghadasa and G. Yushin, Adv. Mater., 2013, 25, 6625-6632.

3. S. I. White, R. M. Mutiso, P. M. Vora, D. Jahnke, S. Hsu, J. M. Kikkawa, J. Li, J. E. Fischer and K. I. Winey, Adv. Funct. Mater., 2010, 20, 2709-2716.

4. R. D. Farahani, H. Dalir, V. L. Borgne, L. A. Gautier, M. A. E. Khakani, M. Lévesque and D. Therriault, Nanotechnology, 2012, 23, 085502.

5. L. Lu, J. Liu, Y. Hu, Y. Zhang, H. Randriamahazaka and W. Chen, Adv. Mater., 2012, 24, 4317-4321.

6. M. Mahmoodi, M. Arjmand, U. Sundararaj and S. Park, Carbon, 2012, 50, 1455-1464.

7. M. F. De Volder, S. H. Tawfick, R. H. Baughman and A. J. Hart, Science, 2013, 339, 535-539.

8. A. K.-T. Lau and D. Hui, Composites Part B: Engineering, 2002, 33, 263-277.

9. B. Kumar, M. Castro and J. F. Feller, Sens. Actuators, B, 2012, 161, 621-628.

10. D. R. Kauffman and A. Star, Angew. Chem. Int. Ed., 2008, 47, 6550-6570.

11. Alamusi, Y. Li, N. Hu, L. Wu, W. Yuan, X. Peng, B. Gu, C. Chang, Y. Liu, H. Ning, J. Li, Surina, S. Atobe and H. Fukunaga, Nanotechnology, 2013, 24, 455501.

12. Y. Wang, A. X. Wang, Y. Wang, M. K. Chyu and Q.-M. Wang, Sens. Actuators, A, 2013, 199, 265-271.

13. S. J. Park, O. S. Kwon and J. Jang, Chem. Commun., 2013, 49, 4673-4675.

14. T. Villmow, S. Pegel, P. Pötschke and G. Heinrich, Polymer, 2011, 52, 2276-2285.

15. K. Kobashi, T. Villmow, T. Andres, L. Häußler and P. Pötschke, Smart Mater. Struct., 2009, 18, 035008.

16. P. Pötschke, T. Andres, T. Villmow, S. Pegel, H. Brünig, K. Kobashi, D. Fischer and L. Häussler, Composites Science and Technology, 2010, 70, 343-349.

17. R. Rentenberger, A. Cayla, T. Villmow, D. Jehnichen, C. Campagne, M. Rochery, E. Devaux and P. Pötschke, Sens. Actuators, B, 2011, 160, 22-31.

18. T. Villmow, S. Pegel, A. John, R. Rentenberger and P. Pötschke, Mater. Today, 2011, 14, 340-345.

19. T. Villmow, A. John, P. Pötschke and G. Heinrich, Polymer, 2012, 53, 2908-2918.

20. K. Kobashi, T. Villmow, T. Andres and P. Pötschke, Sens. Actuators, B, 2008, 134, 787-795.

21. P. Pötschke, K. Kobashi, T. Villmow, T. Andres, M. C. Paiva and J. A. Covas, Compos. Sci. Technol., 2011, 71, 1451-1460.

22. D. Therriault, R. F. Shepherd, S. R. White and Jennifer A. Lewis, Advanced Materials, 2005, 17, 395-399.

23. Jennifer A. Lewis, Advanced Functional Materials, 2006, 16, 2193-2204.

24. L. Lebel, B. Aissa, M. El Khakani and D. Therriault, Advanced Materials, 2010, 22, 592-596.

25. S.-Z. Guo, F. Gosselin, N. Guerin, A.-M. Lanouette, M.-C. Heuzey and D. Therriault, Small, 2013, 9, 4118-4122.

26. S.-Z. Guo, M.-C. Heuzey and D. Therriault, Langmuir, 2014, DOI: 10.1021/la4036425.

27. S. Abbasi, P. J. Carreau, A. Derdouri and M. Moan, Rheologica Acta, 2009, 48, 943-959.

28. F. Du, J. E. Fischer and K. I. Winey, Phys. Rev. B, 2005, 72, 121404.

29. S. Sato, D. Gondo, T. Wada, S. Kanehashi and K. Nagai, J. Appl. Polym. Sci., 2013, 129, 1607-1617.

Nanoscale Accepted Manuscript